Microsystem Technologies 1 (1994) 51–58 © Springer-Verlag 1994

Thermal bubble powered microactuators

Liwei Lin, Albert P. Pisano

Abstract Thermal bubble powered micro mechanical actuators have been successfully demonstrated in working liquids. Micro mechanical plates which function as the mechanical actuators are $70 \times 60 \times 2\ \mu m^3$ in size. They have been fabricated by surface-micromachining technology and suspended 2 μm above the substrate by the supports of cantilever beams. Micro thermal bubbles which are generated by heavily phosphorus doped polysilicon line resistive heaters have been used to lift the mechanical plates in a controllable manner. The typical current required to generate a single, spherical thermal bubble as the actuation source on top of the micro line resistors ($60 \times 2 \times 0.3\ \mu m^3$ in size) is 8.4 mA (80 m Watt) in FC 43 liquid (an inert, dielectrical fluid available from the 3M company). The thermal bubbles have been demonstrated to actuate the mechanical plate perpendicularly to the substrate with a maximum elevation distance of 140 μm and a maximum actuation force of 2 μN. This new actuation mechanism is expected to find applications for micro fluidic devices.

Nomenclature

c_p = specific heat of polysilicon, watt $m^{-1}°C^{-1}$
D = diameter of a thermal bubble without actuator plate on top, m
E_p = Young's Modulus of polysilicon, $N\,m^{-2}$
F_s = thermal conductive shape factor
F_{ap} = bubble force to lift up the actuator plate, N
F_{bubble} = bubble force acting perpendicular to the actuator plate, N
F_{thermo} = thermocapillary force, N
h = thickness of the actuator plate, m
I_{ap} = moment of inertia of the actuator plate, m^4
I_{beam} = moment of inertia of a suspended beam structure, m^4
J = current density, Amp m^{-2}
k_n = thermal conductivity of silicon nitride, watt $m^{-1}°C^{-1}$
k_o = thermal conductivity of silicon dioxide, watt $m^{-1}°C^{-1}$
k_{n+o} = oxide and nitride combined thermal conductivity, watt $m^{-1}°C^{-1}$
k_p = thermal conductivity of polysilicon, watt $m^{-1}°C^{-1}$
k_s = thermal conductivity of silicon substrate, watt $m^{-1}°C^{-1}$
L = length of the micro heater, m
L_{beam} = length of a suspended cantilever beam, m
L_{ap} = length of the actuator plate, m
p_l = pressure of the liquid surrounding the micro bubble, $N\,m^{-2}$
p_v = pressure of the vapor inside the micro bubble, $N\,m^{-2}$
R = resistance of the micro line heater, ohm
r = radius of the micro bubble, m
r_{ap} = the contact circle radius of the bubble and actuator plate, m
T = temperature along the micro line heater, °C
T_{ssmax} = steady state maximum temperature on the micro line heater, °C
T_∞ = ambient (bulk) temperature, °C
T_r = reference temperature in heat equation, °C
t_g = thickness of the gap between actuator plate and ground, m
t_n = thickness of silicon nitride, m
t_o = thickness of silicon dioxide, m
w = width of the micro line heater, m
x = coordinate along the length of the micro line heater, m
z = thickness of the micro line heater, m
α_p = thermal diffusivity of polysilicon, $m^2\ second^{-1}°C^{-1}$
δ_{ap} = vertical deflection at the center of the actuator plate, m
ε = a combined variable term in the heat equation, $°C\,m^{-2}$
ρ_0 = the resistivity of polysilicon at room temperature, ohm-m

Liwei Lin* Albert P. Pisano
Department of Mechanical Engineering,
Berkeley Sensor and Actuator Center,
University of California, Berkeley, CA 94720, U.S.A.

Current address: BEI Electronics, Fremont, CA

The authors would like to thank Prof. V.P. Carey, Mechanical Engineering department, U.C. Berkeley and Dr. A.P. Lee for valuable discussions. The devices were fabricated in the UC Berkeley Microfabrication Laboratory and the FC liquid was provided by 3M company. This work has been supported by Berkeley Sensor and Actuator Center, an NSF/Industry/University Co-operative Research Center.

ρ_p = density of polysilicon, kg m^{-3}
σ_l = the surface tension of the liquid, N m^{-1}
θ_{ap} = deflection angle at the center of the actuator plate, degree
ξ_p = polysilicon temperature resistivity coefficient, °C^{-1}

1 Introduction

Micro devices driven by different mechanisms in air have been successfully demonstrated. These actuation mechanisms include thermal actuation [1], electrostatic force [2, 3], magnetic force [4] and many others. The same mechanisms which have functioned well in air face difficulties in driving micro fluidic devices due to the high drag imposed by fluid viscosity. Although several driving mechanisms in liquid have already been demonstrated, they have drawbacks. Piezoelectric pumps [5, 6] and electrohydrodynamic pumps [7] require high driving voltages (from tens to hundreds of volts) to overcome drag due to fluid viscosity effect. Ultrasonic lamb wave devices [8], although requiring only a small input source (a few volts), generate low output forces.

A powerful driving mechanism in liquid environment can be easily generated by nucleating thermal bubbles [9]. The printer manufacturers (as exemplified by Hewlett-Packard and Canon) have already demonstrated one usage of the powerful thermal micro bubbles by ejecting ink droplets for printing [10]. Although the pressure generated by the nucleating of micro bubbles has been estimated to be 10 atm [11], to the best knowledge of the authors, this pressure has not been previously used to directly actuate a micro mechanical structure in a direction normal to the substrate. Motion parallel to the substrate has been demonstrated by researchers recently at Sandia National Laboratories [12].

This paper presents the novel usage of the micro thermal bubbles for direct mechanical actuation. It is the first time that the micro bubbles have been used to mechanically lift micro mechanical structures in working liquids. Both the nucleation of the micro thermal bubbles and the controllability of the micro mechanical actuators have been demonstrated. The electro-thermal model of the line resistive heater, the mechanical model of the actuators and the pressure and force model of the thermal bubbles are presented.

2 Design and fabrication

2.1 Design

The thermal bubble powered actuator consists two parts as illustrated in Fig. 1, a micro line resistor and a mechanically liftable actuator plate. The polysilicon micro line resistor is placed underneath the actuator plate and functions as a micro resistive heater to generate micro bubbles. The actuator plate is suspended above the substrate by a cantilever beam and is free to move perpendicularly. By passing a sufficient power through the micro line resistor via the two driving pads, a micro bubble can be generated and used to mechanically lift the actuator plate.

The dimensions of the micro line resistor are 60 μm long, 2 μm wide and 0.3 μm thick. These values been chosen

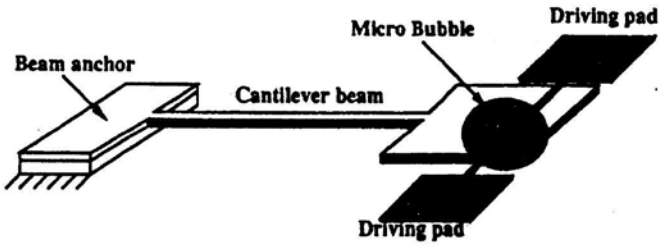

Fig. 1. Schematic diagram of a bubble powered microactuator. The actuator plate is drawn as transparent to show the micro bubble and heater underneath it.

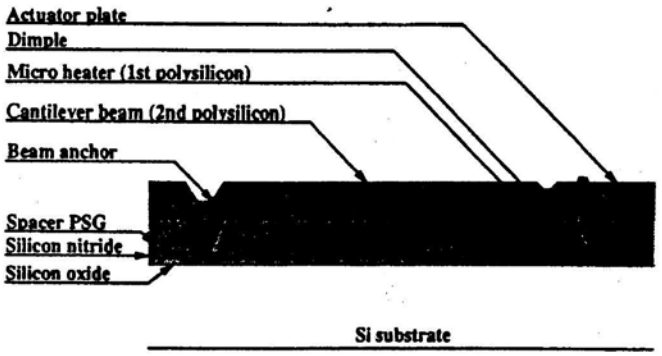

Fig. 2. Fabrication process for the bubble powered microactuator

emperically based on the previous design experience [13]. The actuator plate has the dimension of 60 × 70 × 2 μm^3 in order to fully cover the micro bubble generated during the normal operation. The separation distance between heater and plate has been determined by the thickness of the sacrificial PSG layer (2 μm for a standard surface-micromachining process [3].) The only structure that has design variations in this paper is the cantilever beam which has width ranging from 2 to 10 μm and length ranging from 200 to 400 μm. Both the cantilever beams and the actuator plates have the same thickness of 2 μm.

2.2 Micromachining processes

The cross section view shown in Fig. 2 illustrates the process sequence. Wet oxidation of silicon wafers is first performed to create a 0.55 μm thick silicon dioxide layer. A LPCVD silicon-rich, low-stress nitride deposition of 0.45 μm thick is followed. Both the silicon dioxide layer and the silicon nitride layer serve as the thermal barrier layers underneath the micro line resistive heater. Both the line resistive heaters and the contact pads are made of LPCVD *insitu* phosphorus-doped polysilicon of 0.3 μm thick which is deposited and plasma etched on top of the silicon nitride layer. A 2 μm thick of LPCVD phosphosilicate glass (PSG) is deposited on top of the line resistive heaters to create the suspension spacing for the actuator plates and cantilever beams. Dimples which have been designed to reduce the sticking problem in the final releasing process are defined. They have the sizes of 2 × 2 μm^2 and 1 μm deep into the PSG layer by a timed, 5:1 BHF wet etch. The anchors of the cantilever beams are defined in the same PSG layer and plasma etched down to the first polysilicon layer. A 2 μm thick LPCVD

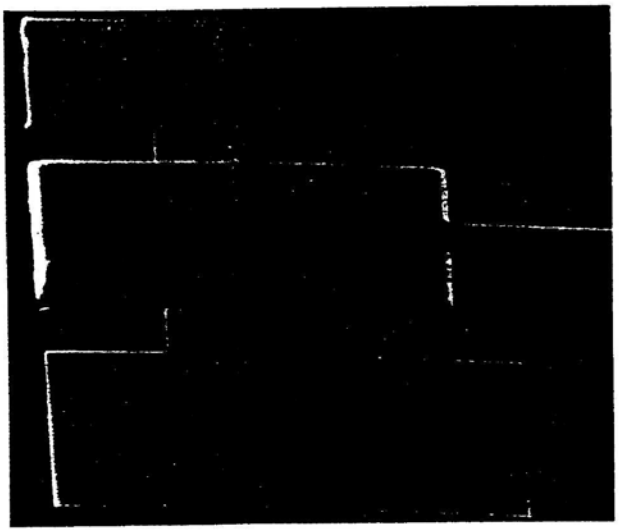

Fig. 3. SEM microphoto of a fabricated microactuator. The actuator plate, micro line resistor, driving pads and two dimples can be seen in the photo

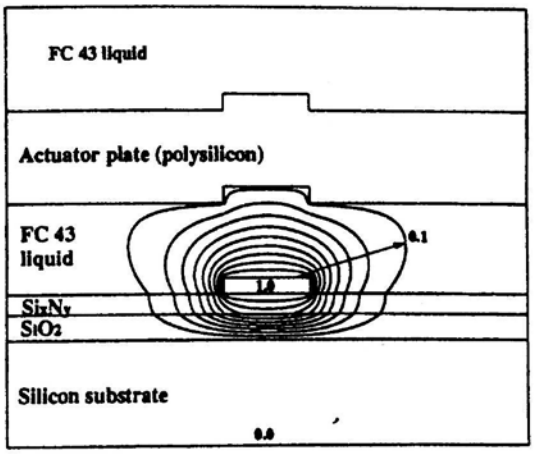

Fig. 4. Cross section view of the isothermal lines for a 2 μm wide micro line resistor under the actuator plate and immersed in FC 43

polysilicon is deposited to form the structures of cantilever beams and actuator plates by a CCl_2 plasma etch. Finally, sacrificial PSG is removed in 10:1 HF for 90 mins and the whole wafer is rinsed in DI water and dried out under an IR lamp. Figure 3 shows the SEM microphoto of the fabricated device including the actuator plate, two dimples, two driving pads, and a portion of the cantilever beam.

3
Theoretical modeling

3.1
Micro line resistor electrothermal model

A lumped, one dimensional electrothermal model can be derived for the micro line resistor by the law of energy conservation [9]. The second order partial differential heat equation is derived as:

$$\frac{\partial^2 T}{\partial x^2}=\frac{1}{\alpha_p}\frac{\partial T}{\partial t}+\varepsilon(T-T_r) \tag{1}$$

in which T is the temperature along the micro line heater, t is time, α_p is the thermal diffusivity of polysilicon. Both ε and T_r are parameters that are functions of heater dimensions and thermal properties of the insulation layers. These variables are expressed as:

$$\alpha_p=\frac{k_p}{c_p\rho_p} \tag{2}$$

$$\varepsilon=\frac{k_{n+o}F_s}{k_p z(t_o+t_n)}-\frac{J^2\rho_0\xi_p}{k_p} \tag{3}$$

$$T_r=\frac{k_{n+o}F_s T_\infty}{k_p z(t_o+t_n)\varepsilon}+\frac{J^2\rho_0}{k_p\varepsilon}-\frac{J^2\rho_0\xi_p}{k_p\varepsilon}, \tag{4}$$

Where k_{n+o} is the combined thermal conductivity of silicon dioxide layer and silicon nitride layer underneath the micro line resistor. It can be expressed as:

$$k_{n+o}=\frac{k_n k_o(t_n+t_o)}{k_o t_n+k_n t_o} \tag{5}$$

An excessive flux shape factor, F_s, is used in the equations to account for the excessive heat conduction losses to the substrate and to the environment. This factor is defined as the total heat flux out of the micro line resistor per unit length divided by the heat flux going directly under the resistor width only.

$$F_s=\frac{\text{total heat flux per unit length}}{\dfrac{wk_{n+o}(T-T_\infty)}{t_o+t_n}} \tag{6}$$

No analytical solution can be found in this case and a finite element analysis is performed to simulate this number. An electrostatic finite element solver [14] is used in this case based on the fact that the electrostatic field is analogy to the thermal field. The simulation result is shown in Fig. 4 where isothermal lines are plotted around the cross section of the micro resistor. It is noticed that most heat transfer occurred in a small confined region under the actuator plate and the highest temperature is at the micro line resistor. The excessive flux shape factor, F_s, is simulated to be 1.64 in this case.

The maximum temperature occurs at the middle point for the micro line resistor underneath the actuator plate. It can be expressed as:

$$T(x)_{ssmax}=T_r-(T_r-T_\infty)\frac{1}{\cosh\left(\sqrt{\varepsilon}\dfrac{L}{2}\right)} \tag{7}$$

This equation gives important information about the bubble formation temperature on the micro line resistors.

3.2
Cantilever beam and actuator plate mechanical response

It is assumed that the total bubble force, F_{ap}, acts as a concentrated force at the center of the actuator plate as seen in Fig. 5. By applying beam theory with variable cross section areas

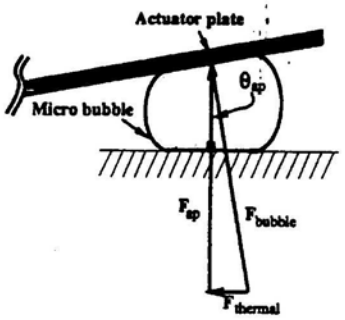

Fig. 5. Schematic force diagram of a micro bubble acting underneath the actuator plate

[15], the deflection, δ_{ap}, and the rotation, θ_{ap}, at the center of the actuator plate are derived:

$$\delta_{ap} = F_{ap}\left[\left(\frac{L_{beam}^3 + L_{beam}L_{ap}}{2E_pI_{beam}}\right)\left(\frac{2L_{beam}}{3} + L_{ap}\right) + \left(\frac{L_{beam}L_{ap}}{2E_pI_{beam}}\right)(L_{beam}^3 + L_{ap}) + \left(\frac{L_{ap}^3}{3E_pI_{ap}}\right)\right] \quad (8)$$

$$\theta_{ap} = F_{ap}\left[\left(\frac{L_{beam}^2 + 2L_{beam}L_{ap}}{2E_pI_{beam}}\right) + \left(\frac{L_{ap}^2}{2E_pI_{ap}}\right)\right] \quad (9)$$

where L_{beam} is the length of the Cantilever beam, L_{ap} is the half length of the actuator plate and I_{beam}, I_{ap} are the moment of inertia of the beam and the actuator plate respectively. The deflection of the actuator plate is measured under a microscope such that the force of the micro bubble can be calculated according to Eq. (8). The rotation of the actuator can be derived subsequently by using Eq. (9).

A side force due to thermocapillary effects can be caused by large deflections as seen in Fig. 5. Due to the rotation of the plate, the micro bubble is pushed away from the center to the edge and a restoring force caused by thermocapillary effect is induced. This termocapillary force can be expressed as:

$$F_{thermo} = F_{ap}\tan\theta_{ap} \quad (10)$$

This force is the result of the strong temperature differences in a small region and is called the Marangoni effect [16, 9], the thermocapillary force induced by gradients of surface tension in the liquid.

3.3
Micro bubble pressure response

The pressure created by a stand along micro bubble in a pool of liquid is illustrated in Fig. 6. The vapor pressure inside this spherical bubble is equal to the liquid pressure outside the bubble plus the interfacial surface tension according to the Young-Laplace equation [17]:

$$p_v = p_l + 2\frac{\sigma_l}{r} \quad (11)$$

where p_v and p_l are vapor and liquid pressures respectively, r is the radius of a spherical micro bubble and σ_l is the surface tension of the liquid.

To analyze the bubble pressure underneath the actuator plate as seen in Fig. 7, a first order model is constructed. The bubble

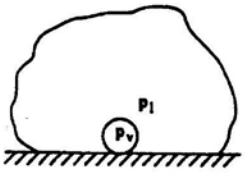

Fig. 6. Schematic diagram of a micro bubble in liquid

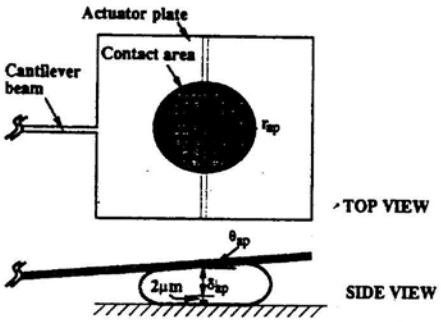

Fig. 7. Top and Side view of a micro bubble underneath the actuator plate

actuation force is expressed by extending the Young-Laplace equation:

$$F_{ab} = \left(\frac{\sigma_l}{0.5(\delta_{ap} + t_g)} + \frac{\sigma_l}{r_{ap}}\right)(\pi r_{ap}^2) \quad (12)$$

where δ_{ap} is the measured deflection, t_g is the thickness of original gap between actuator plate and the ground, σ_l is the surface tension of the surrounding liquid, and r_{ap} is the radius of the contact circle between the bubble and the plate as seen in Fig. 7.

Unfortunately, the contact radius, r_{ap}, is not observable for the current micro actuators which use a 2 μm thick opaque polysilicon actuator plate. Two measurable quantities are used to estimate r_{ap}. For a given value of input power, the bubble diameter, D, is measured without the actuator plate on top. Then, for the same input power, the deflection of the actuator plate, δ_{ap} is measured. The total bubble area in each case is assumed to be the same. This preliminary estimation is based on the assumption that under a fixed input power, the micro line resistor gives the same evaporation rate both before and after the thermal bubble is squeezed by the actuator plate. Since an equilibrium state is reached during the experiments, the condensation rate of the vapor thermal bubbles can be assumed to be about the same. According to a first order approximation [18], the condensation process is directly proportional to the total surface area of the micro bubble such that the total area of a micro bubble is equal to the total area of a squeezed bubble under the actuator plate:

$$\pi D^2 = 2(\pi r_{ap}^2) + \frac{\pi(\delta_{ap} + t_g)}{2}(2\pi r_{ap}) \quad (13)$$

Where D is the measured micro bubble diameter without actuator plate on top and δ_{ap} is the measured deflection of actuator plate under the same input current. The value of r_{ap} under different input currents is derived by measuring D and δ_{ap}.

Table 1. Experimental data for micro bubble diameter and input current.

Current (mA)	5.3	5.5	5.7	5.9	6.1	6.3
Diameter (± 2 μm)	34	45	55	64	72	76

4 Experiments and discussions

4.1 Experiment setup

All the experiments are observed under a probe station equipped with a TV camera to record the results. Experimental data are collected with the FC43 liquid deposited in a puddle of 5 mm deep. Since the FC liquid has the property of high wettability, it wets the 2 μm gap between the actuator plate and the substrate without any problem.

Both DC and AC inputs have been used to generate micro bubbles. AC input to the polysilicon line resistor results in that at frequencies lower than 5 Hz, the actuator plate responds to the input but at double the input frequency due to the natural rectification resistor heating performed on AC current. However, as the frequencies increase, the range of the displacement decreases, and when the frequency is larger than 100 Hz the actuator behaves identically to the DC input.

Deionized water as well as ordinary water have been tested. Micro bubbles have been nucleated in both liquids and have actuated the actuator plates. However, during the ordinary water experiments, the bubble forming mechanism seems to be the combination of electrolysis and the phase changes. This electrolysis reaction can be prevented if bonding wires are used to input the power on a remote site and the micro line heaters is protected under a layer of electrically insulated material.

4.2 Thermal and mechanical responses

It is observed that a current of 8.4 mA at a voltage of 10 volts is required to initiate nucleation of the bubble and that the current may later be reduced to control the bubble size and the deflections of the actuator plate. By applying Eq. 1 and the material properties, the corresponding maximum temperature for this bubble nucleation current is calculated to be approximately 257 °C, which is about 93% of the critical temperature (294 °C) for the FC 43 liquid. This result is similar to the results of previous bubble formation studies which were made without the actuator plate on top of the heater [13].

Static displacements of the actuator plate are measured by using an optical microscope with focus/defocus techniques at the center of the actuator plate. A typical waiting time of 1 to 5 seconds is needed before the micro bubble and the deflection stabilize after increasing or decreasing the input power. As the micro bubble grows, the rotation of the actuator plates pushes the micro bubbles to the edges of the plates and the bubble eventually escapes. The final deflections before the micro bubble departing are recorded as the maximum deflections and the corresponding forces are calculated according to Eq. (8). The departing angles are then calculated by using Eq. (9) which also reveals the corresponding thermal capillary forces by applying Eq. (10).

All the results from 12 different bubble powered microactuators are summarized in Table 2 in an order of the stiffness of the different cantilever beams. It is noticed that some of the deflections are out of the linear region and for these cases the corresponding forces and angles are not calculated. In general, stiffer beams allow smaller maximum deflections, smaller departing angles and smaller thermocapillary forces. The maximum deflection from this set of devices is 140 μm by the $400 \times 2 \times 2$ beam and the maximum departing angle (in the linear region) is 14 degrees by the $400 \times 4 \times 2$ beam. The maximum force generated by the micro bubble is 2 μN by the $200 \times 20 \times 2$ beam and the maximum thermocapillary force is 0.224 μN by the $400 \times 4 \times 2$ beam.

4.3 Micro bubble pressure response

In order to estimate micro thermal bubble pressure responses, both the thermal bubble sizes without the actuator plate and the deflections of the actuator plates are recorded. The bubble size versus input current is first measured as listed in Table 1. They have been measured by using a micro heater of $60 \times 2 \times 0.3$ μm³ in dimension without the actuator plate on top. The deflection versus current for the series of 400 μm long beams is then measured as shown in Fig. 8. There are two input current

Table 2. Experimental data for 12 different micro bubble powered actuators

Structure types (μm³)	Spring constant $\left(\frac{\mu N}{\mu m}\right)$	Maximum deflection (± 1 μm)	Maximum force (μm)	Departing angle (degree)	Thermocapillary force (μN)
$400 \times 2 \times 2$	140	0.006	***	***	***
$400 \times 4 \times 2$	71	0.013	0.90	14.0	0.224
$300 \times 2 \times 2$	75	0.014	***	***	***
$400 \times 6 \times 2$	53	0.019	1.01	10.4	0.185
$300 \times 4 \times 2$	52	0.027	1.44	13.2	0.337
$400 \times 10 \times 2$	35	0.031	1.11	6.88	0.134
$200 \times 2 \times 2$	55	0.040	***	***	***
$300 \times 10 \times 2$	14	0.069	0.97	3.50	0.059
$200 \times 4 \times 2$	23	0.080	1.85	8.26	0.268
$200 \times 6 \times 2$	16	0.121	1.93	1.75	0.059
$300 \times 20 \times 2$	12	0.138	1.66	3.06	0.089
$200 \times 20 \times 2$	5	0.402	2.01	1.81	0.064

*** nonlinear region

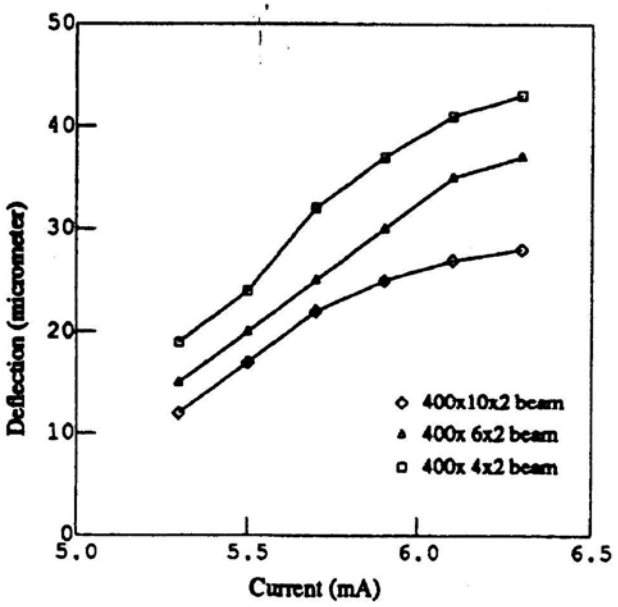

Fig. 8. Experimental data of the actuator displacement versus input current

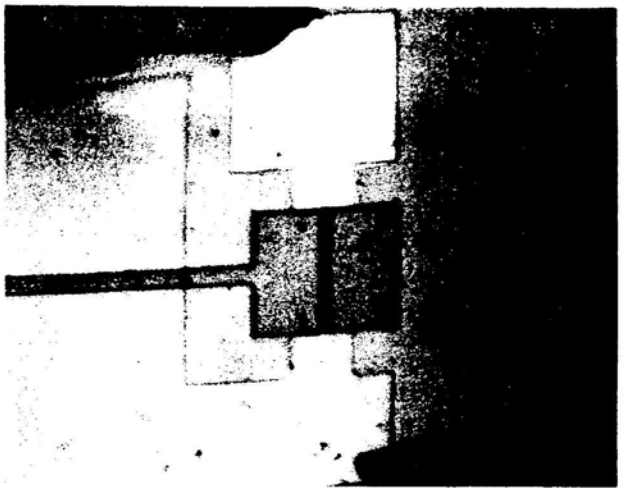

Fig. 9. Three stages of actuations: No input current

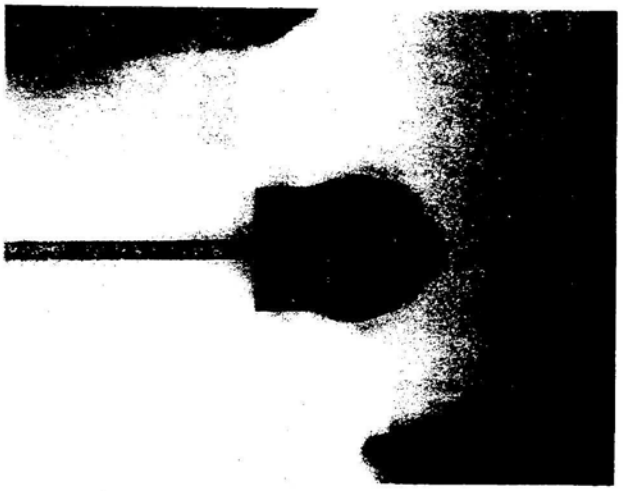

Fig. 10. Input current is 5.9 mA and a bubble is formed under the plate

regions without any records. For the input current under 5.3 mA, the bubble shrinks and disappears. For the input current greater than 6.3 mA, the bubble size will uncontrollably increase and drift to the outside edge of the actuator plate, from which the bubble subsequently escapes.

The actuation forces can be calculated by using the beam formula of Eq. (8). They are illustrated as the solid lines in Fig. 12. The symbols in Fig. 12 are calculated by using the bubble pressure model of Eq. (12) and an experimental surface tension value of 2.4 dynes/cm has been used as the result of best data fit. The theoretical surface tension has not been derived since the temperature field around the thermal bubble is out of the scope of this paper. However, the average temperature around the thermal bubble is expected to be near the boiling temperature of the liquid. As expected, the experimental surface tension of 2.4 dynes/cm is much lower than the room temperature value, 16 dynes/cm, for FC 43 [19].

4.4
Three stages of actuation

Three stages of the actuation have been observed and illustrated in Figs. 9 to 11. In Fig. 9, no power is applied to the heater and the actuator plate remains at the original position. After applying a current of 8.4 mA, a micro bubble forms. The diameter of the very first bubble formed keeps growing in an unstable manner but can be stablized by reducing the input current. The bubble size can be stably controlled as shown in Fig. 10, where the bubble lifts the actuator plate up to a height of 25 μm under an input current of 5.9 mA. The bubble cannot be clearly seen underneath the actuator plate which is made of by 2 μm thick of polysilicon but the lifting of the plate can be detected by observing the color change of the plate and the deflection can be measured by focus/refocus under the microscope. This scheme is demonstrated in Fig. 10 where the focus is set at the center of the actuator plate and the ground plane underneath is out of focus and vague in the photograph. After further increasing the input power, the bubble grows larger and is observed to drift to the outside edge of the actuator plate. At the third stage, the first bubble escapes from beneath the actuator plate and is pulled back the center of the actuator plate due to two effects. One is the strong Marangoni effect, which states the bubbles will move to the hot liquid area due to the surface tension differences. The other is the abrupt pressure drop on top of the plate during the plate downward movement as the bubble escapes [18]. There are two bubbles existing at this stage, one above and one below the actuator plate at the same time. This transient stage has been observed and shown in Fig. 11. The micro bubble attached to the top of the actuator plate will gradually condense if the input power is lowered.

4.5
Limitation of the model

4.5.1
Mechanical response

The model of cantilever beam is established under the assumption that micro bubble reacts as a concentrated force at

Fig. 11. The first bubble escapes and is lodged on top of the plate, while a second bubble forms beneath the plate

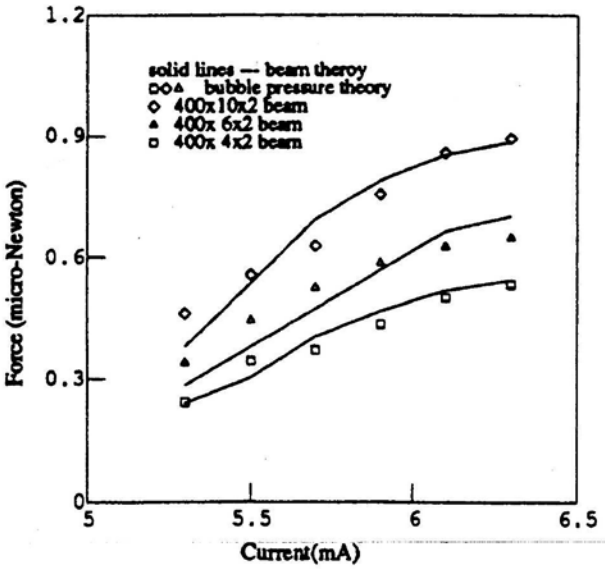

Fig. 12. Calculated actuation forces (beam theory and bubble pressure theory) versus input current

the center of the plate. However, for large deflections, the actuator plate rotates and pushes the micro bubble outward. Not only does the value of L_{ap} change as the bubble moves away from the center point of the actuator plate, but also the small deflection beam theory is no longer valid.

4.5.2
Bubble pressure model

The bubble pressure model used the first order assumption that the total micro bubble area remains unchanged before and after the actuator plate sequeezes the micro bubble. This is not exactly what happens in reality since the existence of the actuator plate changes the heat transfer environment. Nevertheless, the current model provides first order information about the bubble pressure and the surface tension.

A transparent actuator plate could be built for the next generation of bubble actuators to measure the actual dimension of the contact radius between the micro bubble and the actuator plate. Furthermore, the temperature field surrounding the bubble should be analyzed by a full three-dimensional model to further understand the thermodynamic behavior of the thermal bubbles and its actuation power to the micro mechanical structures.

5
Conclusions

Microelectromechanical actuators based on thermal bubble actuation are demonstrated. This new class of microactuator presents a novel usage of thermal bubbles to directly actuate structures normal to the substrate and is expected to find applications in micro fluid devices. A four mask surface micromachining process is used,to fabricate heavily phosphorus doped polysilicon line resistive heaters and cantilever-type actuators on a same chip. The electrically non-conducting liquid, Fluorinert FC 43 (a product of 3M company) as well as DI and ordinary water have all been successfully used as the working liquids. With a typical current of 8.4 mA for a $60 \times 2 \times 0.32\ \mu m^3$ polysilicon resistor, thermal bubbles are generated in FC 43 liquid. These thermal bubbles are used as the actuation sources to lift the cantilever microactuators with different beam dimensions. A maximum vertical deflection of 140 μm by a $400 \times 2 \times 2$ cantilever beam actuator and a maximum force of 2 μN by a $200 \times 20 \times 2$ cantilever beam have been achieved.

The local thermocapillary forces can be measured by using this microactuator. It is found that a maximum thermocapillary force of 0.224 μN on a $400 \times 4 \times 2$ beam actuator is induced by the Marangoni effect during the experiments. The local surface tension surround the resistive heater may also be measured by this microactuator. The value for FC 43 liquid has been estimated to be 2.4 dynes/cm by experimental best data fit. Furthermore, three stages of actuations have been observed including two micro bubbles exist on top and bottom of the actuator plate at the same time.

References

1. Riethmuller, W.; Benecke, W. "Thermally excited silicon microactuators", IEEE Trans. on Electron Devices, ED-35: 758–762, June 1988.
2. Petersen, K.E. "Micromechanical membrane switches on silicon", *IBM J. Res. Develop*, 23: 376–385, 1979.
3. Tang, W.C.; Nguyen, T.C.H.; Howe, R.T. "Laterally driven polysilicon resonat microstructures", Sensors and Actuators, 20: 25–32, 1989.
4. Guckel, H.; Christenson, T.R.; Skrobis, K.J.; Jung, T.S.; Klein, J.; Hartojo, K.V.; Widjaja, I. "A first functional current excited planar rotational magnetic micromotor", Proceedings of IEEE Electro Mechanical Systems (MEMS93), pages 7–11, 1993.
5. Van Lintel, H.T.G.; Van Deptol, F.C.M.; Bouwstra, S. "A piezoelectric micropump based on micromachining of silicon", Sensors and Actuators, 15: 153–167, 1988.
6. Esashi, M.; Shoji, S.; Nakano, A. "Normally closed microvalve and micropump fabricated on a silicon wafer". Sensors and Actuators, 20: 163–169, Nov. 1989.
7. Bart, S.F.; Tavrow, L.S.; Mehregany, M.; Lang, J.H. "Microfabricated Electrohydrodynamic pumps", Sensors and Actuators A-Physical 21: 193–197, 1990.
8. Moroney, R.M.; White, R.M.; Howe, R.T. "Microtransport induced by ultrasonic lamb waves", Applied Physics Letters, 59: 774–776, 1991.
9. Lin, L.; Pisano, A.P. "Bubble Forming on a Micro Line Heater", Proceedings of ASME Winter Annual Meeting, Micromechanical Sensors, Actuators and Systems, DSC-32: 147–163, Dec. 1991.

10. Nielsen, N.J. "History of think jet printerhead development", HP Journal, 36(5): 4–10, May 1985.
11. Allen, R.R.; Meyer, J.D.; Knight, W.R. "Thermodynamics and hydrodynamics of thermal ink jets", HP Journal, 36(5): 21–27, May 1985.
12. Sniegowski, J.J. "A micro actuation mechanism based on liquid-vapor surface tension", Digest of late news of Transducers'93, International Conference on Solid-State Sensors and Actuators, pages 12–13, 1993.
13. Lin, L.; Pisano, A.P.; Lee, A.P. "Microbubble powered actuator", Digest of Transducers'91, International Conference on Solid-State Sensors and Actuators, pages 1041–1044, 1991.
14. Ansoft Corp. Maxwell Solver, 4 Station Square, 660 Commerce Court Building, Pittsburgh, PA, 15219. v. 4.33.
15. Beer F.B.; Johnston, E.R. Mechanics of Materials, McGraw-Hill Book Co., New York, 1981.
16. Scriven, L.E.; Sternling, C.V. "The Marangoni Effects", Nature, 187: 186–188, 1960.
17. Collier, J.G. Convective Boiling and Condensation, McGraw-Hill Book Co., New York, 2nd edition, 1981.
18. Carey, V.P. "Personal communication", University of California at Berkeley, Department of Mechanical Engineering, 1991.
19. Fluorinert Electronic Liquids. Product manual, 3M Industrial Chemical Production Division, St. Paul, MN 55144, 1991.